Int. J. Heat Mass Transfer. Vol. 27, No. 5, pp. 697–704, 1984
Printed in Great Britain

0017–9310/84 $3.00 + 0.00

NATURAL CONVECTION EFFECTS IN THE CONTINUOUS CASTING OF A HORIZONTAL CYLINDER

L. S. YAO
Department of Mechanical and Aerospace Engineering, Arizona State University, Tempe, AZ 85287, U.S.A.

(*Received* 8 *May* 1983 *and in revised form* 19 *August* 1983)

Abstract—The effects of natural convection along the interface between two phases in the continuous casting of a horizontal cylinder are studied. Due to natural convection, the solidification rate along the bottom of a horizontal cylinder is shown to be faster than that along the top. The solidification rate grows downstream as $z^{5/2}$ (z being the axial coordinate) due to the natural convection, and is not aximuthally uniform. This conclusion is an important extension over previous work which considered only conduction and showed a solidification rate which increased as $z^{1/2}$.

NOMENCLATURE

a	radius of the cylinder, Fig. 1
A	resolidification constant due to conduction, equation (7)
B	resolidification constant due to natural convection, equation (7)
f	stream functions, equation (8)
g	gravitational acceleration
Gr	Grashof number
h_s	temperature function, equation (17)
k	thermal conductivity
p, P	pressure
Pe	Peclet number, equation (5)
Pr	Prandtl number
r, ϕ, z	coordinates
R	location of the interface between two phases
Re	Reynolds number, equation (3)
T	temperature
u, v, w	velocity components, Fig. 1
y	boundary-layer coordinate, equation (5).

Greek symbols

α	thermal diffusivity
β	thermal expansion coefficient
ζ	$y/\sqrt{(2z)}$, equation (8)
η	coordinate, equation (16b)
θ, Θ	dimensionless temperature, equations (1) and (16a).

Subscripts

l	molten pool
m	interface
1	outer surface of the cylinder
s	solid
z	derivative with respect to z
ϕ	derivative with respect to ϕ.

Superscripts

$\bar{}$	dimensional quantities
$'$	derivative with respect to appropriate independent variable.

1. INTRODUCTION

CONTINUOUS casting has been a research topic for many years, and its importance has been repeatedly addressed [1–8]. Furthermore, the basic heat transfer mechanism in continuous casting is shared by different heat transfer problems such as thermally developing flows [2, 10], conduction controlled rewetting [9], and the freezing process in pipe flows. Most of the previous work concentrates on the mechanism of heat conduction inside a moving slab or a moving rod, and ignores the natural convection effect.

A typical continuous casting is shown in Fig. 1. A molten material, usually several degrees above the solidification temperature, is pulled out of a large chamber, and passes through a cooling mold. The mold is continuously cooled by circulating cooling water through passages in the mold walls. Due to this energy removal from the molten material a solid crust is formed. If some of the core is still liquid at the exit of the mold, the strength of the solidified crust must be sufficient to contain the remaining liquid and permit continuous withdrawal of the casting. The detailed processes of continuous casting vary for different materials, some of them are desribed in refs. [1–8].

Kroeger and Ostrach [3] studied the natural convection effect on metal casting along the vertical direction. In this paper, an asymptotic solution is presented which demonstrates the effect of natural convection on the continuous casting of a *horizontal* cylinder. A coordinate transformation method is applied to overcome the difficulty associated with the fact that the interface between the molten and the resolidified phases must be determined as a part of the solution.

In Section 2, three radial regions are considered: (a) the molten core moves away from the chamber which contains the molten material (usually several degrees above the solidification temperature); (b) the solidified solid crust whose outside temperature T_1 is assumed constant and is several degrees below the phase-change temperature, and (c) in between these two regions, the liquid is cooled from T_i to T_m, solidification

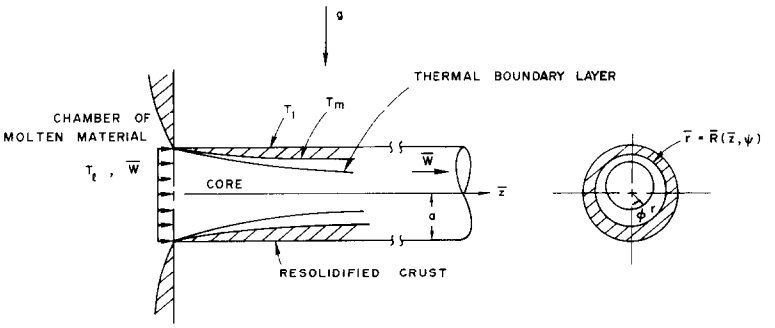

FIG. 1. Physical model and coordinates.

temperature. This is a thermal boundary layer where mixed convection has to be considered. As a first attempt at solving this complex conjugate problem in this particular geometry, an asymptotic analysis is carried out. The asymptotic solution is valid only in a small axial region near the exit of the chamber, but does reveal the important physics of continuous casting processes, and identifies the relevant parameters which are needed to improve future designs. Even though the region in which the asymptotic solution can be applied is small, the formulation presented is valid for the complete casting process and can be solved numerically. The advantages of the current formulation are due to the method of coordinate transformation. Three radial regions are transformed into three regular shapes: two concentric annuli and one circular cylinder. Therefore, previously developed numerical methods can be readily applied to the transformed equations without worrying about the *unknown* interface between the thermal boundary layer and the solidified crust. Furthermore, the separated formulations for the molten core and the thermal boundary layer allow one to use a coarse grid for the molten core and a fine grid for the thermal boundary layer where a large temperature gradient exists without introducing numerical instability. This formulation also avoids the difficulty associated with limited computer storage which is still a concern for three-dimensional (3-D) problems such as the one considered here. The present solution shows that the resolidification process is faster along the bottom of the cylinder due to the effects of natural convection.

2. GOVERNING EQUATIONS AND SOLUTIONS

2.1. *Molten material*

Near the exit of the chamber containing molten material, Fig. 1, the characteristic length is the radius of the exit a and the velocities of the liquid phase are scaled by the uniform velocity $\bar{W}$ at the exit. The pressure is nondimensionalized by $\rho\bar{W}^2$ where ρ is the density. The dimensionless radial coordinate is defined as

$$r = \frac{\bar{r}}{\bar{R}(z,\phi)} = \frac{\bar{r}}{aR(z,\phi)}, \tag{1a}$$

and the dimensionless temperature is

$$\Theta = \frac{T_l - T}{T_l - T_m}, \tag{1b}$$

where T_l is the temperature of the molten material in the chamber and T_m is the solidification temperature. Then the dimensionless equations of motion and energy with the Boussinesq approximation become

$$\frac{DW}{Dz} + \frac{\partial U}{\partial r} + \frac{U}{r} + \frac{1}{r}\frac{DV}{D\phi} = 0, \tag{2a}$$

$$W\frac{DW}{Dz} + U\frac{\partial W}{\partial r} + \frac{V}{r}\frac{DW}{D\phi} = -\frac{DP}{Dz} + \frac{1}{Re}\left(\frac{\partial^2 W}{\partial r^2} + \frac{1}{r}\frac{\partial W}{\partial r} + \frac{1}{r^2}\frac{D^2W}{D\phi^2} + \frac{D^2W}{Dz^2}\right), \tag{2b}$$

$$W\frac{DU}{Dz} + U\frac{\partial U}{\partial r} + \frac{V}{r}\frac{DU}{D\phi} - \frac{V^2}{r} = -\frac{\partial P}{\partial r} - \varepsilon(\Theta_c - \Theta)\cos\phi + \frac{1}{Re} \times \left(\frac{\partial^2 U}{\partial r^2} + \frac{1}{r}\frac{\partial U}{\partial r} + \frac{1}{r^2}\frac{D^2U}{D\phi^2} + \frac{D^2U}{Dz^2} - \frac{U}{r^2} - \frac{2}{r^2}\frac{DV}{D\phi}\right), \tag{2c}$$

$$W\frac{DV}{Dz} + U\frac{\partial V}{\partial r} + \frac{V}{r}\frac{DV}{D\phi} + \frac{UV}{r} = -\frac{1}{r}\frac{DP}{D\phi} + \varepsilon(\Theta_c - \Theta)\sin\phi + \frac{1}{Re} \times \left(\frac{\partial^2 V}{\partial r^2} + \frac{1}{r}\frac{\partial V}{\partial r} + \frac{1}{r^2}\frac{D^2U}{D\phi^2} + \frac{\partial^2 V}{\partial z^2} - \frac{V}{r^2} + \frac{2}{r^2}\frac{DU}{D\phi}\right), \tag{2d}$$

$$W\frac{D\Theta}{Dz} + U\frac{\partial\Theta}{\partial r} + \frac{V}{r}\frac{D\Theta}{D\phi} = \frac{1}{Pr\,Re} \times \left(\frac{\partial^2\Theta}{\partial r^2} + \frac{1}{r}\frac{\partial\Theta}{\partial r}\frac{1}{r^2}\frac{D^2\Theta}{D\phi^2} + \frac{D^2W}{Dz^2}\right), \tag{2e}$$

where Θ_c is the value of Θ at $r = 0$

$$\frac{D}{Dz} = \frac{\partial}{\partial z} - \frac{r}{R}\frac{\partial R}{\partial z}\frac{\partial}{\partial r}, \tag{3a}$$

$$\frac{D}{D\phi} = \frac{\partial}{\partial \phi} - \frac{r}{R}\frac{\partial R}{\partial \phi}\frac{\partial}{\partial r}, \tag{3b}$$

and

$$Re = \frac{\bar{W}a}{\nu}, \tag{3c}$$

$$Gr = \frac{\beta g(T_0 - T_m)a^3}{\nu^2}, \tag{3d}$$

$$\varepsilon = \frac{Gr}{Re^2}, \tag{3e}$$

$$Pr = \frac{\nu}{\alpha_l}. \tag{3f}$$

The zero-order solution of equations (2a)–(2e) is simply an undisturbed uniform flow so that

$$W = 1,$$
$$U = V = \Theta = 0, \tag{4}$$
and
$$P = \text{const.}$$

It is obvious that the above solution cannot be applied to the region near the surface of a solidifying cylinder. Near this surface, a thin crust is formed and heat transfer takes place in the liquid phase close to the thin crust. This is a boundary-layer region in which a rapid change occurs. The proper variables for this region are

$$y = Pe^{1/2}\frac{\bar{R} - \bar{r}}{a} = Pe^{1/2}(R - r)$$

(stretched normal coordinate),

$$U = -Pe^{1/2}(U - R_z W - R_\phi V), \tag{5}$$
$$v = V, \quad \theta = \Theta, \quad \text{etc.}$$

where $Pe = Pr\ Re$ is the Peclet number and the subscript denotes partial derivative. Equation (5) shows that the thickness of the thermal boundary layer near the thin crust is of the order of $Pe^{-1/2}$. Substitution of equations (5) into equations (2a)–(2e), after neglecting the smaller order terms, gives

$$\frac{\partial w}{\partial z} + \frac{\partial u}{\partial y} + \frac{1}{R - y/\sqrt{Pe}}\left[\frac{\partial v}{\partial \phi} + (R_z w + R_\phi v - u/\sqrt{Pe}) - \sqrt{Pe}(R - 1 - y/\sqrt{Pe})R_\phi \frac{\partial v}{\partial y}\right] = 0, \tag{6a}$$

$$w\frac{\partial w}{\partial z} + u\frac{\partial w}{\partial y} + \frac{v}{R - y/\sqrt{Pe}} \times \left[\frac{\partial w}{\partial \phi} + \sqrt{Pe}(R - 1 - y/\sqrt{Pe})R_\phi \frac{\partial v}{\partial y}\right] = -\left(\frac{\partial P}{\partial z} + \sqrt{Pe}\ R_z \frac{\partial P}{\partial y}\right) + Pr\frac{\partial^2 w}{\partial y^2}, \tag{6b}$$

$$w\frac{\partial v}{\partial z} + u\frac{\partial v}{\partial y} + \frac{v}{R - y/\sqrt{Pe}} \times \left[\frac{\partial v}{\partial \phi} + \sqrt{Pe}(R - 1 - y/\sqrt{Pe})R_\phi \frac{\partial v}{\partial y}\right] = -\frac{1}{R - y/\sqrt{Pe}}\left(\frac{\partial P}{\partial \phi} + \sqrt{Pe}\ R_\phi \frac{\partial P}{\partial y}\right) - \varepsilon\theta \cos\phi + Pr\frac{\partial^2 v}{\partial y^2}, \tag{6c}$$

$$\frac{\partial P}{\partial y} = \frac{1}{\sqrt{Pe}}\left\{\frac{v^2}{R - y/\sqrt{Pe}} + Pr\left[-\frac{2}{R - y/\sqrt{Pe}} \times \left(\frac{\partial v}{\partial \phi} + \sqrt{Pe}\ R_\phi \frac{\partial v}{\partial y}\right)\right] + \varepsilon\theta \sin\phi\right\}, \tag{6d}$$

$$w\frac{\partial \theta}{\partial z} + u\frac{\partial \theta}{\partial y} + \frac{v}{R - y/\sqrt{Pe}} \times \left[\frac{\partial \theta}{\partial \phi} + Pe(R - 1 - y/\sqrt{Pe})R_\phi \frac{\partial \theta}{\partial y}\right] = \frac{\partial^2 \theta}{\partial y^2}. \tag{6e}$$

Near the exit, the *solidified* crust is thin so that R can be expressed as

$$R = 1 - \frac{1}{\sqrt{Pe}}[R_{10}(z) + \varepsilon R_{11}(z, \phi) + \ldots]$$
$$= 1 - \frac{1}{\sqrt{Pe}}[A\sqrt{(2z)} + \varepsilon B \cos\phi(2z)^{5/2} + \ldots]. \tag{7}$$

Here R denotes the distribution of the thin crust (Fig. 1) and can be determined by an energy balance along the interface between the two phases. It should be noted that equations (6a)–(6e) are not limited for a thin crust. Its governing equation will be derived after the heat-conduction solution for the solid has been presented. R_{10} represents the formation of the crust due to conduction and R_{11} is due to the natural convection effect. Both A and B are constants which will be determined in Section 2.3.

The solution of equations (6a)–(6e) can be expanded in terms of the small parameter ε in the following way

$$w = 1 + \varepsilon \cos\phi(2z)^2 f_1'(\zeta) + \ldots, \tag{8a}$$

$$v = \varepsilon \sin\phi(2z) f_2'(\zeta) + \ldots, \tag{8b}$$

$$u = -\varepsilon \cos\phi(2z)^{3/2}[(5f_1 - \zeta f_1') + f_2] + \ldots, \tag{8c}$$

$$\theta = \theta_0(\zeta) + \varepsilon \cos\phi(2z)^2 \theta_1(\zeta) + \ldots, \tag{8d}$$

where $\zeta = y/\sqrt{(2z)}$ and primes denote the derivative with respect to ζ. The effects of natural convection are represented by the terms of $O(\varepsilon)$. Equations (8a)–(8d) clearly show that, even though the natural-convection effects are small near the exit of the chamber, their importance increases rapidly downstream. This is one of the reasons why the asymptotic solution presented, which treats natural convection as an effect of small order, is valid only near the exit of the chamber. Downstream from this small region, the solution of equations (6a)–(6e) must be determined numerically.

The equations for $\theta_0(\zeta)$, θ_1, f_1, and f_2 are

$$\theta_0'' + \zeta\theta_0' = 0, \tag{9}$$

$$Pr\, f_1''' + \zeta f_1''' - 4f_1' = 0, \tag{10a}$$

$$Pr\, f_2''' + \zeta f_2'' - 2f_2' = \theta_0, \tag{10b}$$

$$\theta_1'' + \zeta\theta_1' - 2\theta_1 = -(5f_1 + f_2)\theta_0'. \tag{11}$$

The associated boundary conditions are

$$\zeta = 0: \quad \theta_0 = 1,\ f_1 = f_1' = f_2 = f_2' = 0, \tag{12a}$$

$$\zeta \to \infty: \quad \theta_0, f_1', f_2' \to 0. \tag{12b}$$

The pertinent solutions of equations (9) and (10a) can be easily found; they are

$$\theta_0 = 1 - \frac{2}{\sqrt{\pi}} \int_0^{\zeta} e^{-\zeta^2/2}\, d\zeta = 1 - \operatorname{erf}\left(\frac{\zeta}{\sqrt{2}}\right), \tag{13}$$

and

$$f_1 \equiv 0, \tag{14}$$

where erf denotes the error function. The solutions for f_2' and θ_1 can be expressed in terms of hypergeometric functions, but a direct numerical integration of equations (10b) and (11) can serve the purpose as well. The numerical results are plotted in Figs. 2 and 3 for Pr = 0.1, 1.0, and 10. Their derivatives along the interface between the two phases which are needed to study the formation of the thin crust are listed in Table 1. Physically, f_2' represents the dimensionless azimuthal velocity which is driven by buoyancy. The magnitude of f_2' is larger for a smaller Pr. θ_1 is the modification of the temperature distribution inside the thermal boundary layer due to natural convection. For a smaller Pr, the modification is larger. This indicates that the effect of natural convection is more important for metal castings.

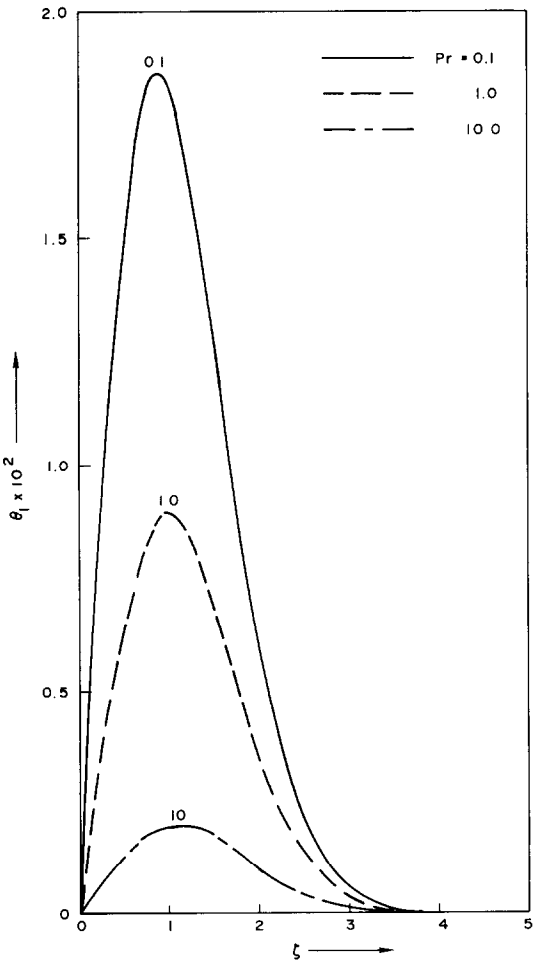

FIG. 2. Second-order liquid temperature.

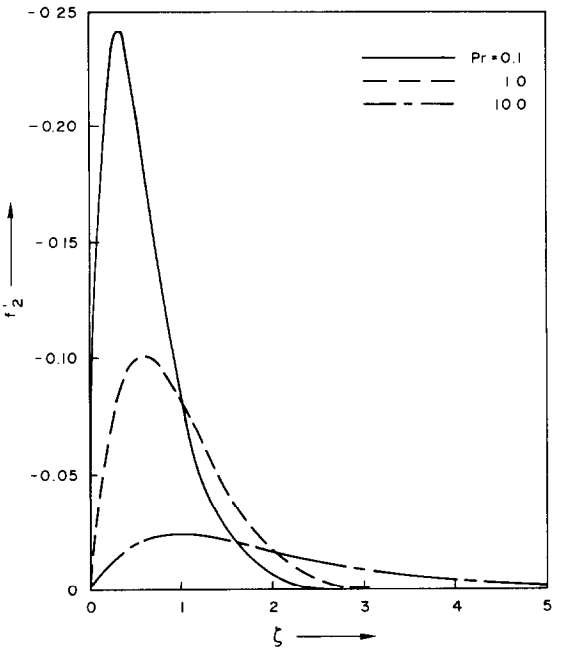

FIG. 3. Secondary flow.

2.2. *Resolidified solid*

Heat conduction through the solid crust determines the rate of resolidification. Since the solid travels at a uniform velocity in the positive x-direction, the dimensionless conduction equation in a moving cylindrical polar coordinate system takes the form

$$\frac{\partial\theta_s}{\partial z} + \frac{R_z}{1-R}\eta\frac{\partial\theta_s}{\partial\eta} = \frac{1}{Pe}\left[\frac{1}{(1-R)^2}\frac{\partial^2\theta_s}{\partial\eta^2} + \frac{1}{1-(1-R)\eta}\frac{1}{1-R}\frac{\partial\theta_s}{\partial\eta} + \frac{1}{1-(1-R)\eta}\left(\frac{\partial}{\partial\phi} + \frac{R_\phi}{1-R}\eta\frac{\partial}{\partial\eta}\right)^2\theta_s + \left(\frac{\partial}{\partial z} + \frac{R_z}{1-R}\eta\frac{\partial}{\partial\eta}\right)^2\theta_s\right], \tag{15}$$

Table 1

Pr	0.1	1.0	10.0
$\theta_1'(0)$	0.03208	0.01314	0.00277
$f_2''(0)$	−1.9161	−0.3989	−0.0606

where the dimensionless temperature is defined as

$$\theta_s = \frac{T - T_1}{T_m - T_1}, \tag{16a}$$

and

$$\eta = \frac{a - \bar{r}}{a - \bar{R}(z, \phi)} = \frac{1 - r}{1 - R}. \tag{16b}$$

The advantages of the coordinate transformations defined in equations (1a), (5) and (16b) have been discussed in refs. [11–14]. The solution of equation (15) which matches with the solution for the liquid phase can be expressed as

$$\theta_s = \frac{\int_0^{\eta} e^{-A^2\eta^2/2}\, d\eta}{\int_0^1 e^{-A^2\eta^2/2}\, d\eta} + \varepsilon \cos \phi (2z)^2 h_s(\eta) + , \ldots . \tag{17}$$

The equation for h_s can be found by substituting equations (7), (13) and (17) into equations (15) and collecting terms of $O(\varepsilon)$, it is

$$h_s'' + A^2\eta h_s' - 4A^2 h_s = -6BA \frac{\eta\, e^{-A^2\eta^2/2}}{\int_0^1 e^{-A^2\eta^2/2}\, D\eta}. \tag{18}$$

The associated boundary conditions are

$$h_s(0) = h_s(1) = 0. \tag{19}$$

2.3. *Interface*

The equation for the interface between the two phases can be determined by an energy balance. In terms of the dimensionless variables defined above, it is

$$\sqrt{Pe}\left[\left(-1 + \frac{R_\phi^2}{R^2} + R_z^2\right)\frac{\partial\theta}{\partial y} - \frac{R_\phi}{R^2}\frac{\partial\theta}{\partial\phi} - R_z \frac{\partial\theta}{\partial z}\right]_{y=0} S_h - \left[\frac{1}{1-R}\left(1 + \frac{R_\phi^2}{R^2}\eta + R_z^2\eta\right) \times \frac{\partial\theta_s}{\partial\eta} - \frac{R_\phi}{R^2}\frac{\partial\theta_s}{\partial\phi} - R_z\frac{\partial\theta_s}{\partial z}\right]_{\eta=1} = \frac{Pe}{S_d}\frac{\partial R}{\partial z}, \tag{20}$$

where

$$S_h = \frac{k_l(T_l - T_m)}{k_s(T_m - T_1)}, \tag{21a}$$

is the superheat factor and

$$S_d = \frac{C_s(T_m - T_1)}{L}\frac{\alpha_s}{\alpha_l} \tag{21b}$$

is the Stefan number. A detailed derivation of equation (20) is described in ref. [12]. Here the time derivative of R in ref. [12] is replaced by $\bar{W}(\partial R/\partial\bar{z})$. Substitution of equation (7) into equation (20) and collecting terms of equal orders yields

$$A^2 + S_d\left[S_h\sqrt{\left(\frac{2}{\pi}\right)}A - \frac{e^{-A^2/2}}{\int_0^1 e^{-A^2\eta^2/2}\, d\eta}\right] = 0, \tag{22}$$

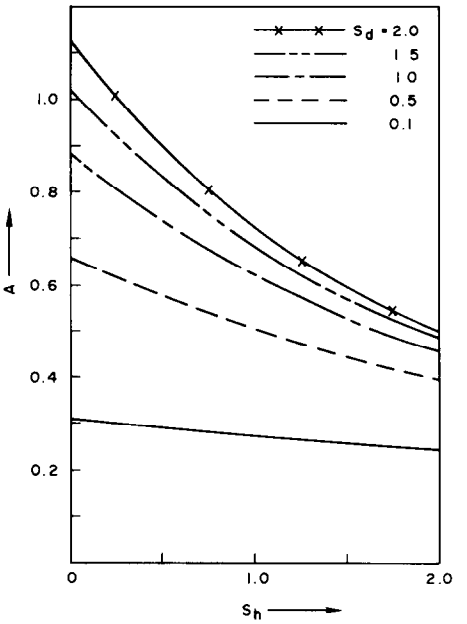

FIG. 4. Frozen solid due to conduction.

and

$$B = S_d \frac{S_h A\theta_1'(0) + h_s'(1)}{5 + (S_d/A)\left(e^{-A^2/2} \Big/ \int_0^1 e^{-A^2\eta^2/2}\right)}. \tag{23}$$

The constant A is determined by solving equation (22) numerically, the results are plotted in Fig. 4. They show that the resolidification due to conduction alone becomes slower when the superheat factor S_h is increased, its rate is faster for materials with larger S_d.

The equations for h_s and B must be solved simultaneously. A typical solution for h_s is given in Fig. 5 for $S_h = S_d = 0.5$ and $Pr = 1$. Values of B and $h_s'(1)$ are plotted in Figs. 6 and 7, respectively. Both B and $h_s'(1)$ have a local maximum when S_h varies. The peak shifts

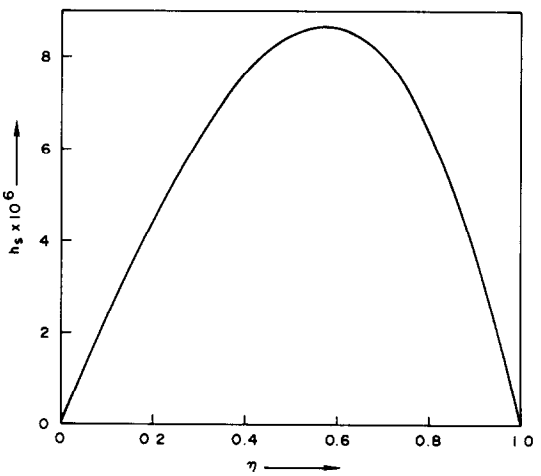

FIG. 5. A typical solution of h_s for $S_d = 0.5$, $S_h = 0.5$ and $Pr = 1.0$.

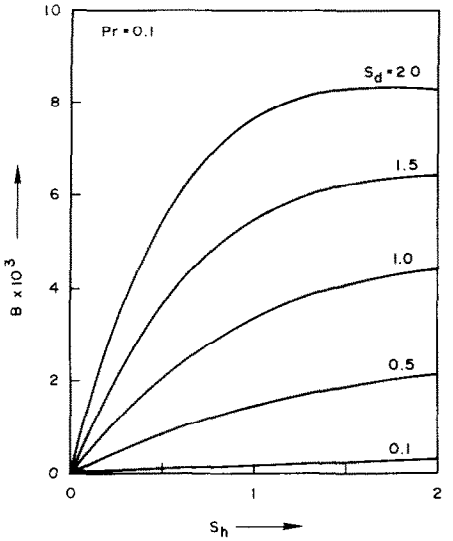

FIG. 6(a). Frozen solid due to convection.

toward smaller S_h for larger S_d. The physical reason for these local maxima is unclear. It should, however, be noted that the decrease of B when S_h increases does not imply that the natural convection effect is weaker. The actual effects of natural convection can be determined by combining B and ε, see equation (7). The increase of B and $h_s'(1)$ with S_d is expected. Since B is positive, solidification is faster along the bottom of the cylinder than along the top. This is due to the natural convection effect in the thermal boundary layer which causes the heat flux out of the liquid phase to be higher along the top of the cylinder. The natural convection effects can be identified by the ratio of R_{11}/R_{10} whose value increase as z^2 downstream.

An important conclusion of the current study can be drawn from equation (7). Previous studies, without considering natural convection, show that the solid crust grows downstream as $z^{1/2}$ with thickness proportional to $1/\sqrt{Pe}$ [see the second term of equation (7)]. On the other hand the proper growth rate of the solidified crust due to natural convection varies as $z^{5/2}$ and is not azimuthally uniform as shown by the third term of equation (7). Therefore, it can be concluded that the natural convection effect grows faster downstream than that due to radial conduction [second term of equation (7)] so that a design without considering natural convection can be in error.

Equations (7), (8) and (17) indicate that the natural-convection effect becomes dominant when εz^2 grows to $O(1)$. Physically, this shows that the asymptotic solution breaks down at a distance of order $a\ Re/Gr^{1/2}$ from the exit of the chamber. In the first axial region $z \sim 1$ and the displacement effects due to the solidified crust and the thermal boundary layer have no influence on the motion of the molten core, since $f_1 \equiv 0$ in

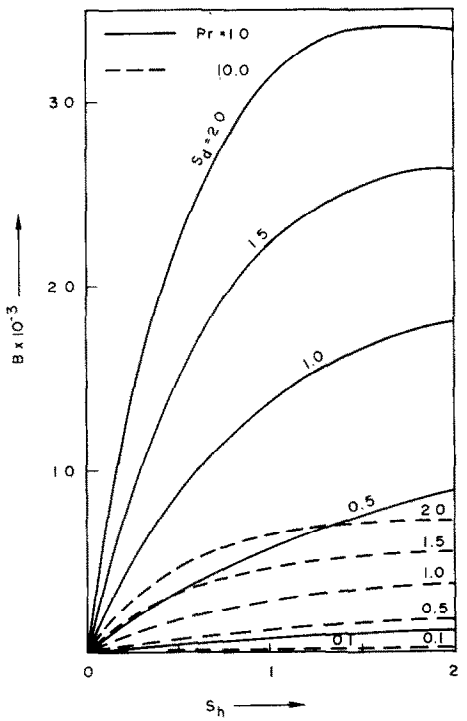

FIG. 6(b). Frozen solid due to convection for Pr = 1.0 and 10.0.

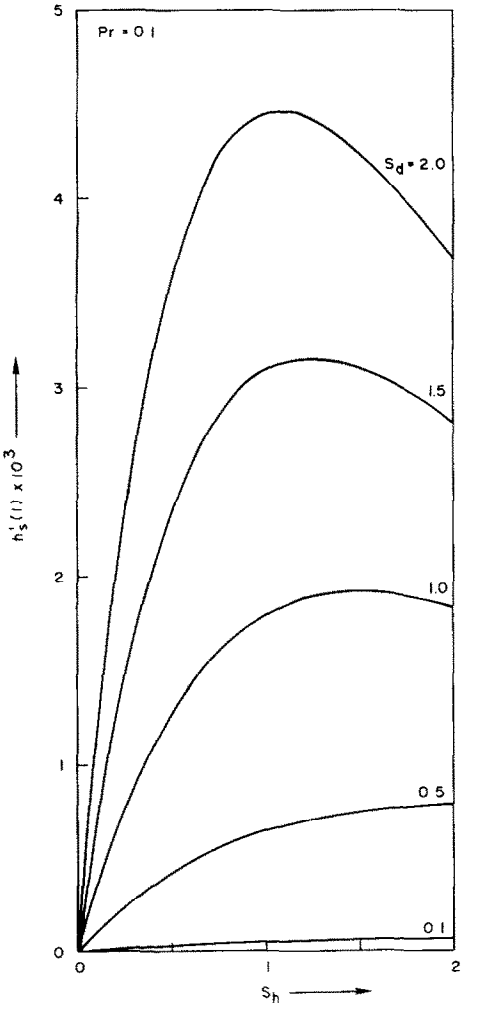

FIG. 7(a). Second-order conduction in solid.

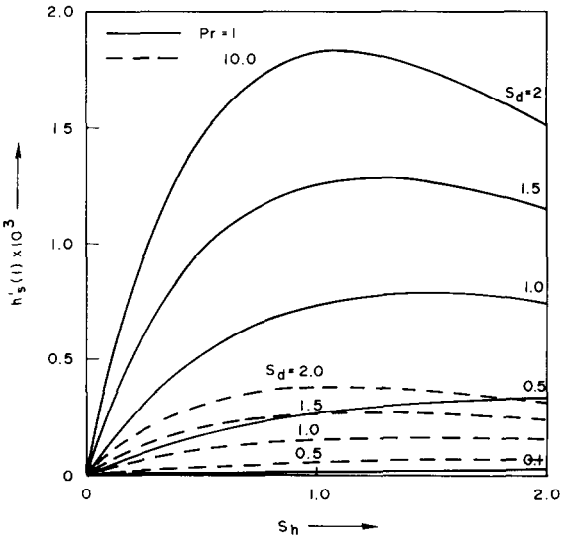

FIG. 7(b). Second-order conduction in solid.

equation (8). Downstream from the first region, the solidified crust grows thicker and becomes asymmetric due to natural convection. The slope, the curvature of the solidified crust, will affect the motion of the molten core [see equations (2) and (3)] in the second axial region where $z \sim \varepsilon^{1/2}$. In this region the thermal boundary layer is 3-D and solutions must be determined numerically. The current formulation for three different radial regions removes the difficulties of applying numerical methods to an unknown and irregular geometry due to the formation of the solid crust.

REFERENCES

1. G. Horvay, The dip-forming process, *J. Heat Transfer* **87**(1), 1–16 (1965).
2. G. Horvay, Temperature distribution in a slab moving from a chamber at one temperature to a chamber at another temperature, *J. Heat Transfer* **83**, 391–402 (1961).
3. P. G. Kroeger and S. Ostrach, The solution of a two-dimensional freezing problem including convection effects in the liquid region, *Int. J. Heat Mass Transfer* **17**, 1191–1207 (1974).
4. R. Siegel, Analysis of solidification interface shape during continuous casting of a slab, *Int. J. Heat Mass Transfer* **21**, 1421–1430 (1978).
5. R. Siegel, Shape of two-dimensional solidification interface during directional solidification by continuous casting, *J. Heat Transfer* **100**, 3–10 (1978).
6. R. Siegel, Cauchy integral method for two-dimensional solidification interface shapes, *Int. J. Heat Mass Transfer* **25**, 975–984 (1982).
7. R. Siegel, Analysis of solidification interface shape resulting from applied sinusoidal heating, *J. Heat Transfer* **104**, 13–18 (1982).
8. J. H. Blackwell and J. R. Ockendon, Exact solution of a Stefan problem relevant to continuous casting, *Int. J. Heat Mass Transfer* **25**, 1059–1060 (1982).
9. C. L. Tien and L. S. Yao, Analysis of conduction-controlled rewetting of a vertical surface, *J. Heat Transfer* **97**, 161–165 (1975).
10. L. S. Yao, C. L. Tien and S. A. Berger, Thermal analysis of a fast-moving slab in two adjacent temperature chambers, *J. Heat Transfer* **98**, 326–329 (1976).
11. L. S. Yao, Analysis of heat transfer in slightly eccentric annuli, *J. Heat Transfer* **102**, 279–284 (1980).
12. L. S. Yao and F. F. Chen, Effects of natural convection in the melted region around a heated horizontal cylinder, *J. Heat Transfer* **102**, 667–672 (1980).
13. J. Prusa and L. S. Yao, Natural convection heat transfer in eccentric annuli, *J. Heat Transfer* **105**, 108–116 (1983).
14. L. S. Yao, Natural convection along a vertical wavy surface, *J. Heat Transfer* **105**, 465–468 (1983).

LES EFFETS DE CONVECTION NATURELLE PENDANT LE MOULAGE D'UN CYLINDRE HORIZONTAL

Résumé—On étudie les effets de la convection naturelle le long de l'interface entre deux phases dans le forgeage continu d'un cylindre horizontal. A cause de la convection naturelle, la solidification à la base du cylindre horizontal est plus rapide qu'au sommet. La vitesse de solidification croît comme $z^{5/3}$ (z étant la coordonnée axiale) et elle n'est pas uniforme azimutalement. Cette conclusion est une extension d'un précédent travail qui considérait seulement la conduction et qui montrait une vitesse de solidification croissant comme $z^{1/3}$.

FREIE KONVEKTIONSEINFLÜSSE BEIM KONTINUIERLICHEN GIESSEN EINES HORIZONTALEN ZYLINDERS

Zusammenfassung—Es wurden die Einflüsse der freien Konvektion an der Phasengrenze beim kontinuierlichen Gießen eines horizontalen Zylinders untersucht. Es wird gezeigt, daß als Folge der freien Konvektion die Erstarrungsgeschwindigkeit an der Unterseite des horizontalen Zylinders größer als an der Oberseite ist. Die Erstarrungsgeschwindigkeit wächst infolge freier Konvektion stromab mit $z^{5/2}$ (wobei z die Koordinate in Achsrichtung ist) und ist in Umfangsrichtung nicht gleichförmig. Dieses Ergebnis stellt eine wichtige Ergänzung früherer Arbeiten dar, bei denen nur die Wärmeleitung berücksichtigt wurde, und denen zufolge die Erstarrungsgeschwindigkeit mit $z^{1/2}$ zunahm.

ЭФФЕКТЫ ЕСТЕСТВЕННОЙ КОНВЕКЦИИ ПРИ НЕПРЕРЫВНОЙ ОТЛИВКЕ ГОРИЗОНТАЛЬНОГО ЦИЛИНДРА

Аннотация—Исследуются эффекты естественной конвекции на границе раздела фаз при непрерывной отливке горизоитального цилиндра. Показано, что из-за влияния естественной конвекции нижняя часть горизонтального цилиндра затвердевает быстрее, чем верхняя. Скорость затвердевания растет вниз по потоку пропорционально $z^{5/2}$ (z—аксиальная координата) в результате влияния естественной конвекции и является азимутально неоднородной. Это новый важный вывод, отличающийся от результатов предыдущей работы, в которой рассматривалась только теплопроводность и где было показано, что скорость затвердевания возрастает пропорционально $z^{1/2}$.